

Supporting Information

Graphene Oxide Coating Core-Shell Silver Sulfide@Mesoporous Silica for Active Targeted Dual-Mode Imaging and Chemo-Photothermal Synergistic Therapy Against Tumor

Yuan-Yang Song^{1‡}, Cheng Li^{1‡}, Xiao-Quan Yang^{1,2‡}, Jie An¹, Kai Cheng¹, Yang Xuan¹, Xue-Meng Shi¹, Meng-Juan Gao¹, Xian-Lin Song², Yuan-Di Zhao^{1,2*}, Wei Chen^{1,2*}

¹ Britton Chance Center for Biomedical Photonics at Wuhan National Laboratory for Optoelectronics – Hubei Bioinformatics & Molecular Imaging Key Laboratory, Collaborative Innovation Center for Biomedical Engineering, College of Life Science and Technology, Huazhong University of Science and Technology, Wuhan 430074, Hubei, P. R. China

² Key Laboratory of Biomedical Photonics (HUST), Ministry of Education, Huazhong University of Science and Technology, Wuhan 430074, Hubei, P. R. China

‡ These authors equally contributed to this article.

* Co-corresponding author. Tel/Fax: +86-27-8779-2202. Email address: zydi@mail.hust.edu.cn (Y.D. Zhao), chen1980wei@mail.hust.edu.cn (W. Chen).

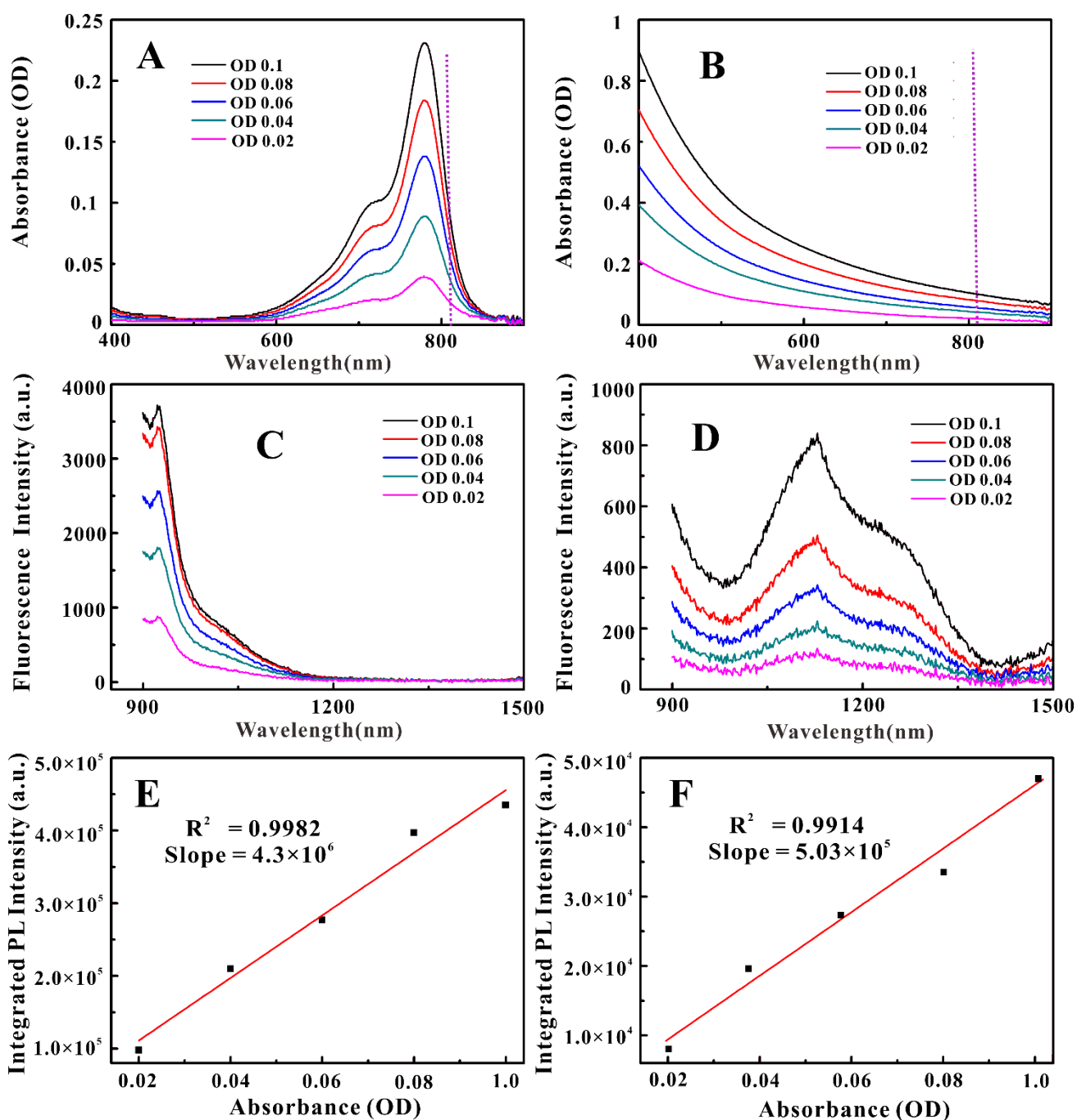


Fig. S1 UV/vis spectra of a series of five solutions of ICG in DMSO (A) and QD@Si/GO-FA (B) at 808 nm; NIR fluorescence spectra of the five ICG (C) and QD@Si/GO-FA solutions (D); the integrated emission intensities of five fluorescence spectra of ICG (E) and QD@Si/GO-FA (F) solutions plotted against the actual absorbances at 808 nm.

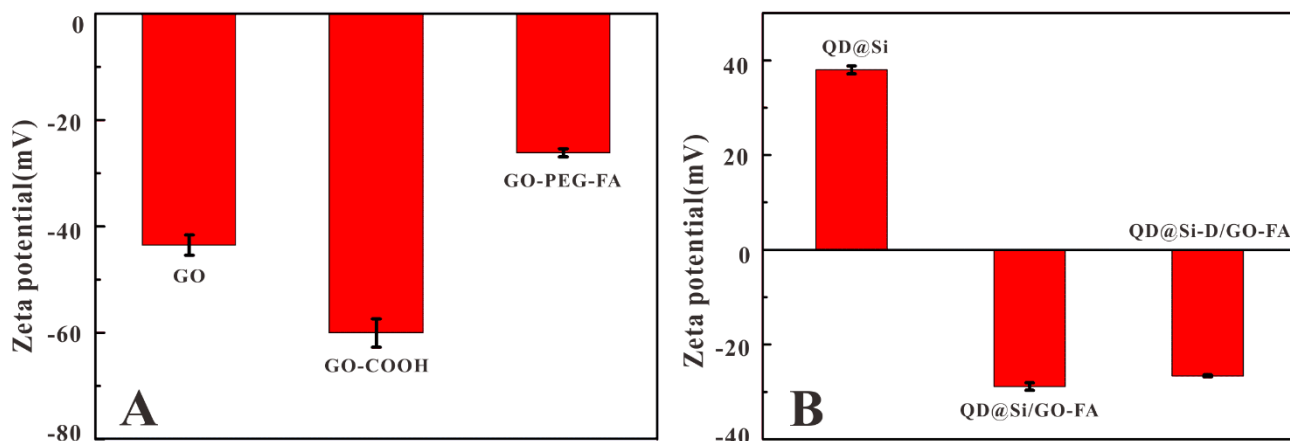


Fig. S2 Zeta potential of GO, GO-COOH and GO-PEG-FA (A); zeta potential of QD@Si, QD@Si/GO-FA and QD@Si-D/GO-FA (B).

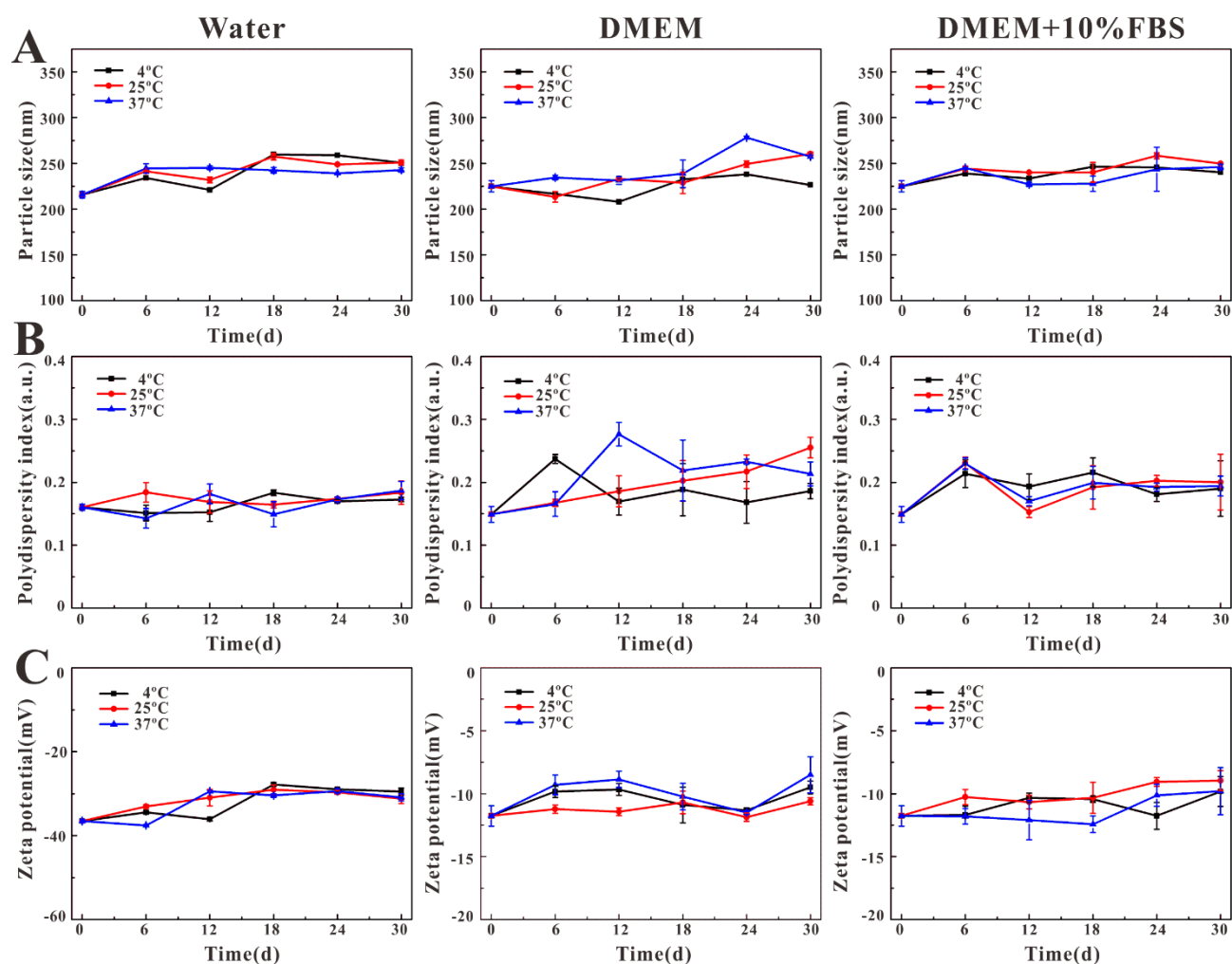


Fig. S3 Hydration particle size (A), PDI (B) and zeta potential (C) of QD@Si/GO-FA dispersed in different dispersions at 4, 25 and 37 °C over time.

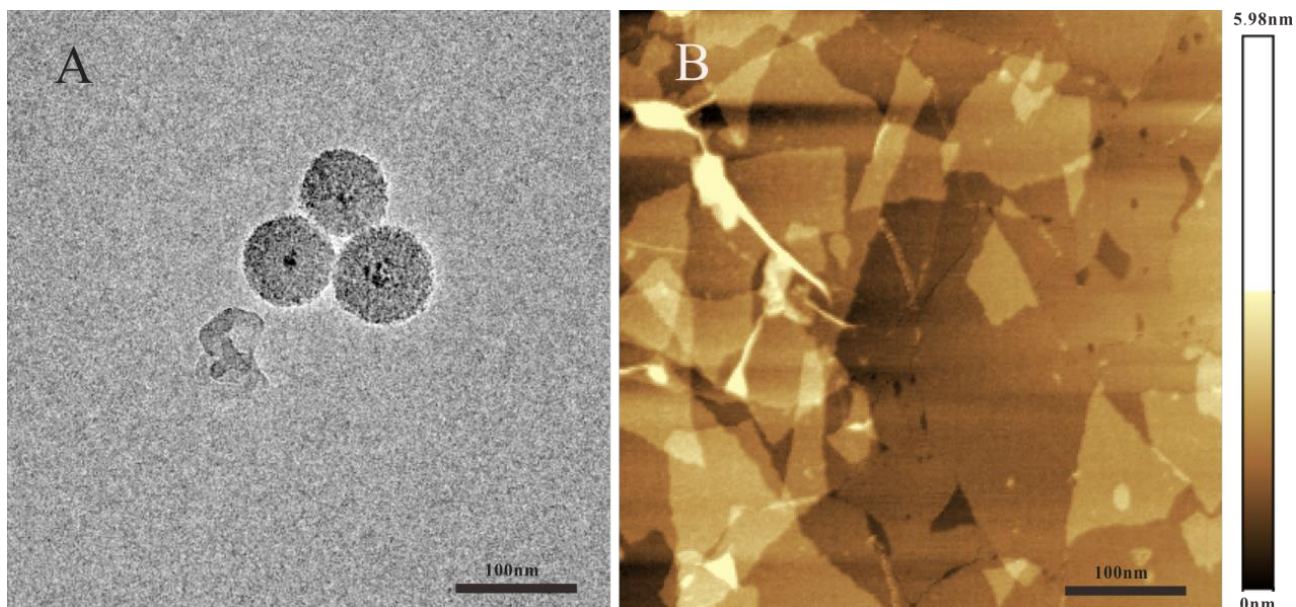


Fig. S4 TEM image of QD@Si/GO-FA after laser irradiation (A); AFM image of GO (B).

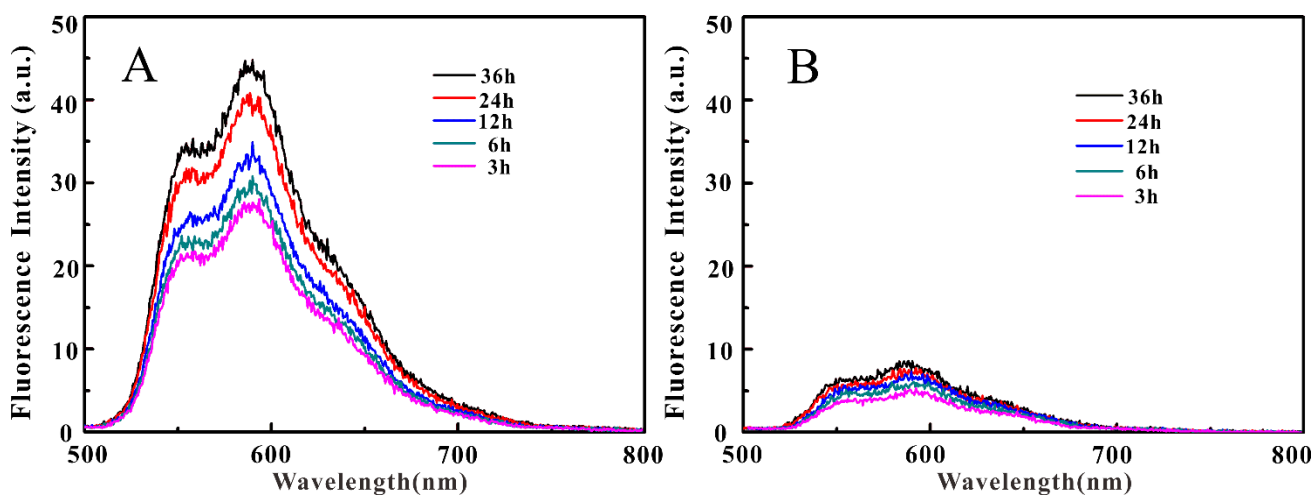


Fig. S5 The fluorescence intensity of cumulative drug release from QD@Si-D/GO-FA in PBS with (A) or without laser (B) for 7 min.

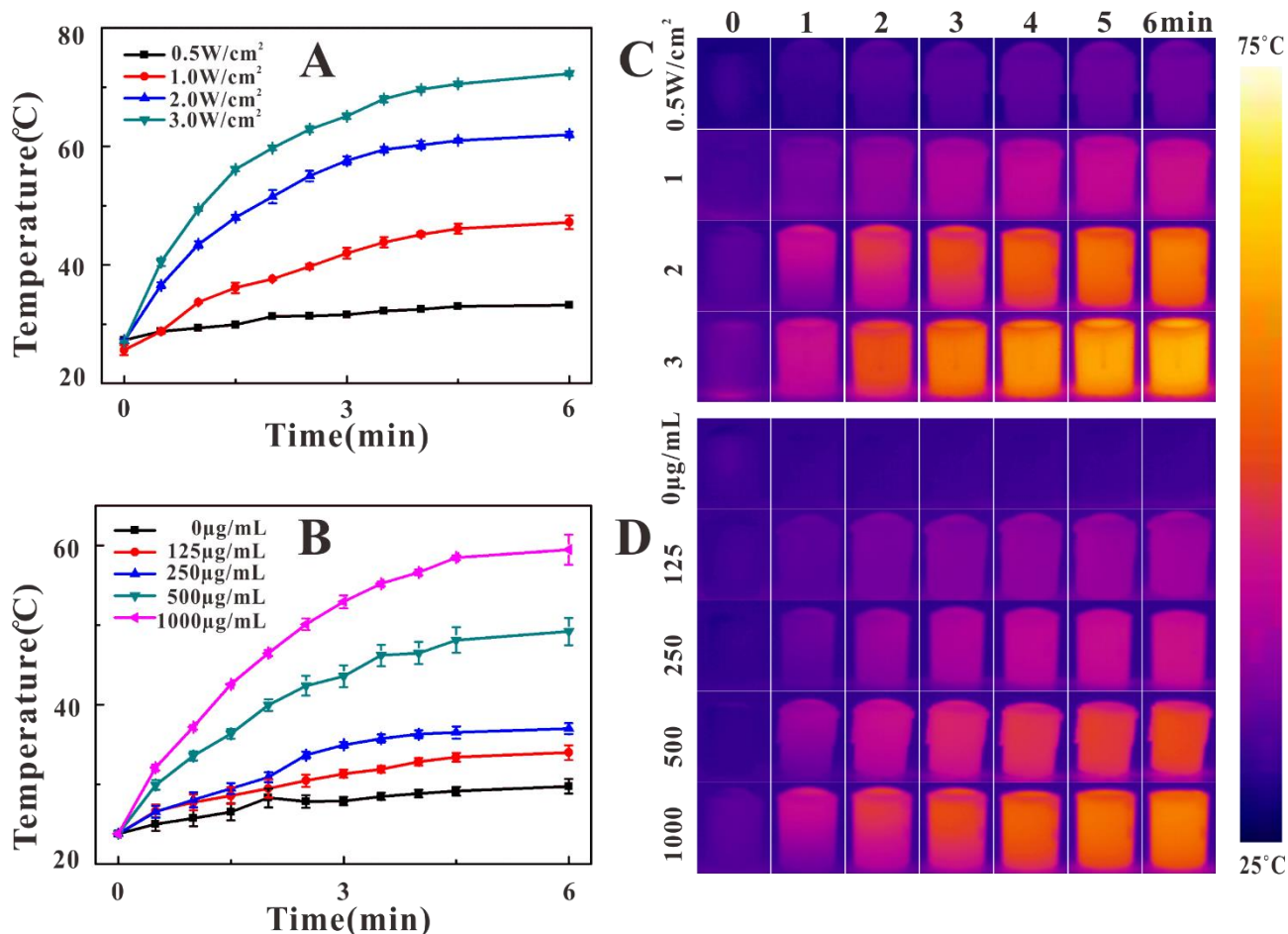


Fig. S6 Temperature elevation (A) and thermal imaging (C) of QD@Si/GO-FA at different laser powers; temperature elevation (B) and thermal imaging (D) of QD@Si/GO-FA under 808 nm laser (2 W cm^{-2}) with different concentrations.

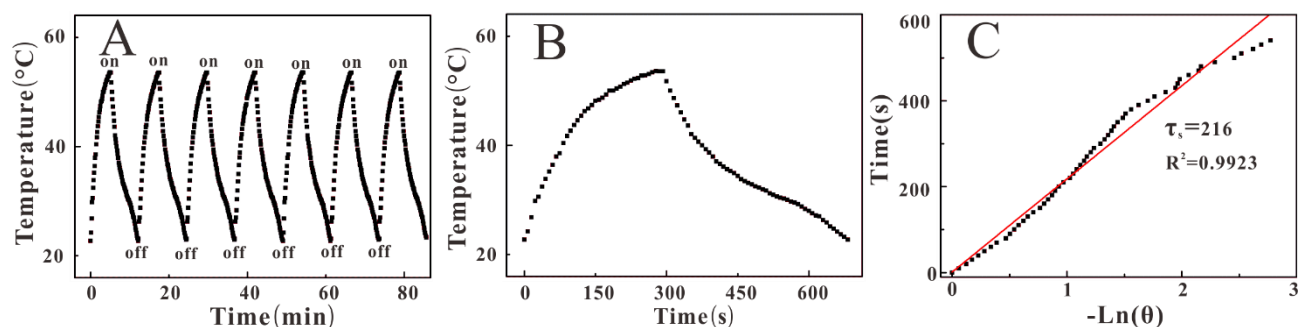


Fig. S7 Temperature elevation of QD@Si/GO-FA dispersed in $300 \mu\text{L}$ water ($500 \mu\text{g mL}^{-1}$) over six laser on/off cycles under NIR laser irradiation (A); photothermal effect of probe irradiated by 808 nm laser (2 W cm^{-2}) turned off after irradiation for 300 s (B); plot of cooling time vs negative natural logarithm of the driving force temperature obtained from the cooling stage (C).

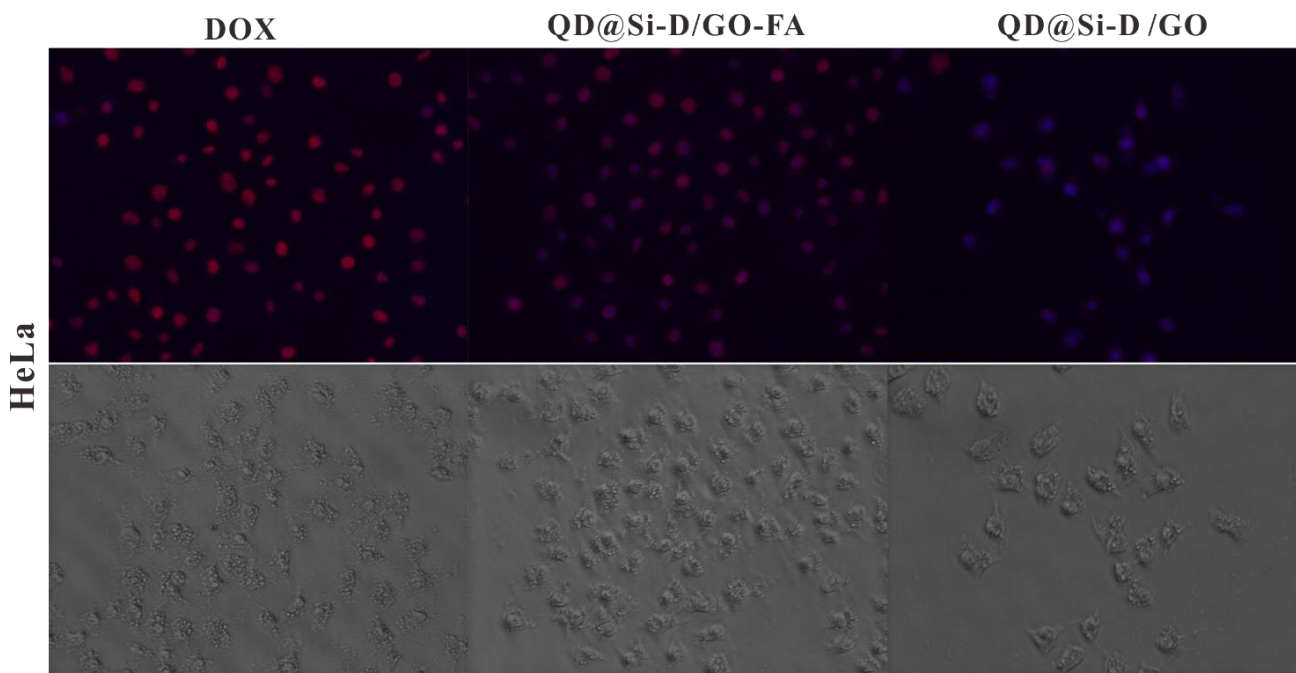


Fig. S8 FL of HeLa cells incubated with DOX, QD@Si-D/GO-FA and QD@Si-D/GO, respectively.

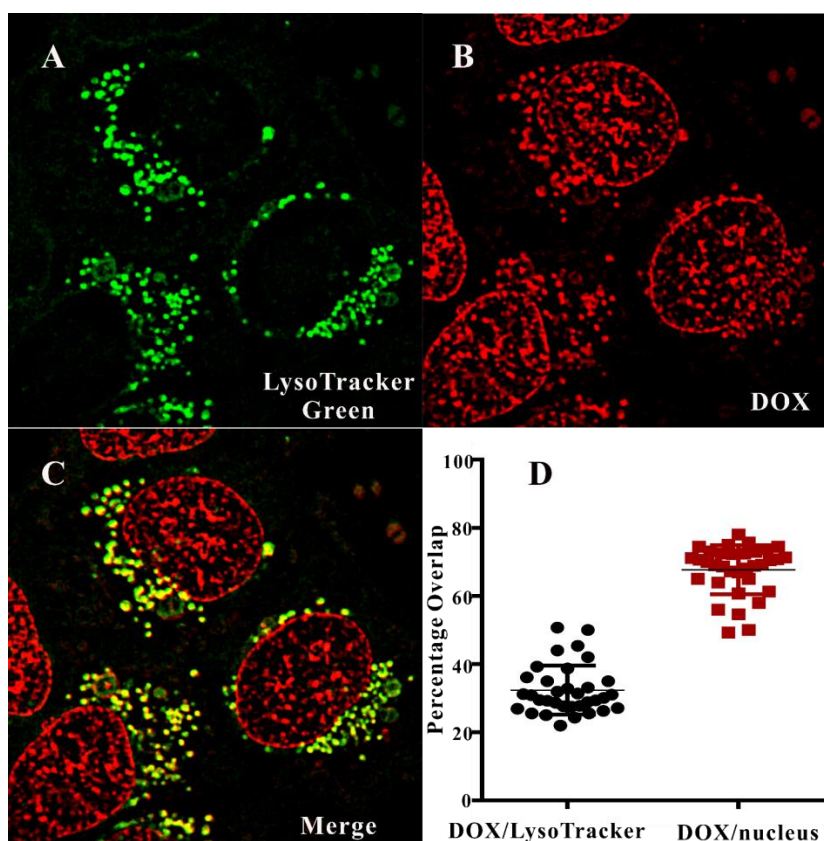


Fig. S9 Confocal images of controlled-release behaviors of QD@Si-D/GO-FA after being treated with HeLa cells for 4 h, upon NIR irradiation with a power density of 2 W cm^{-2} for 5 min. LysoTracker green (green fluorescence) was used to stain the lysosomes. Cells were imaged using a $100\times$ oil-immersion objective(A-C). The percentages of colocalization of DOX with LysoTracker Green (Left) and Nucleus (Right) were analyzed and plotted. The error bars represent the Mean \pm SD of cells (n=26) in each group (D).

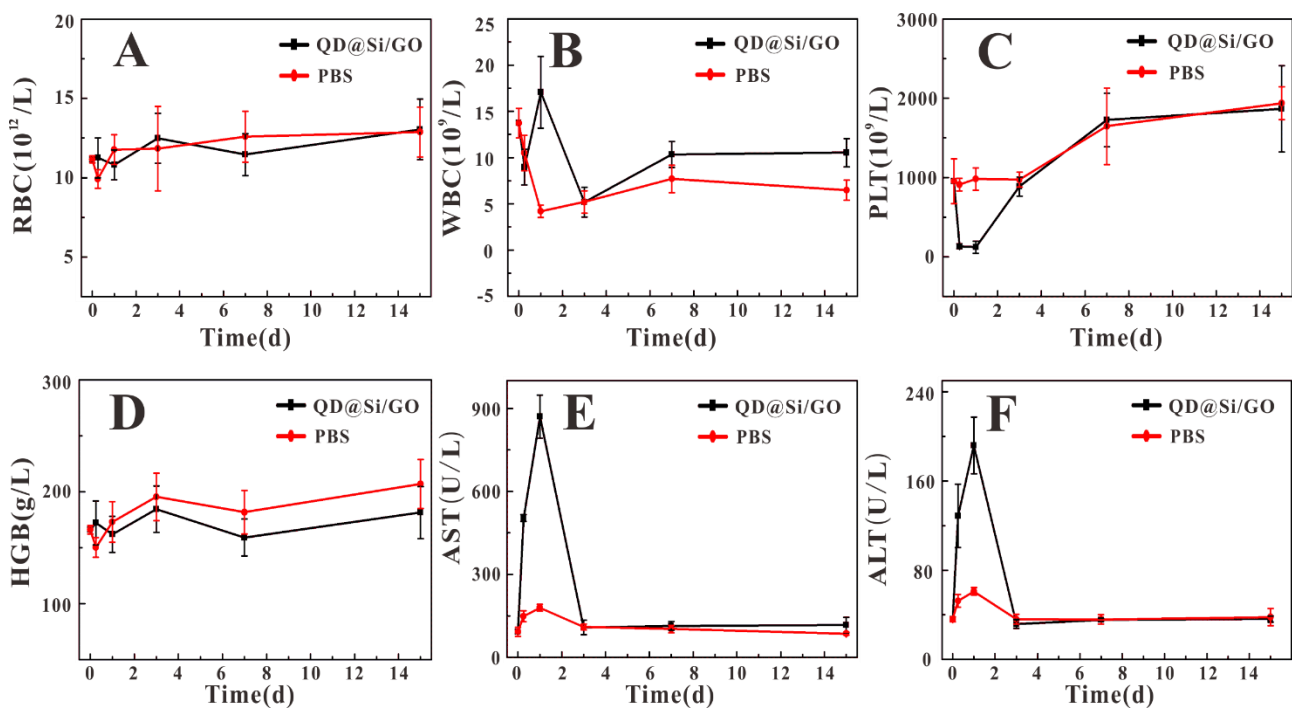


Fig. S10 Blood and liver enzyme analysis of mice injected with QD@Si/GO: RBC (A), WBC (B), PLT (C), HGB (D), AST (E) and ALT (F); n = 5.

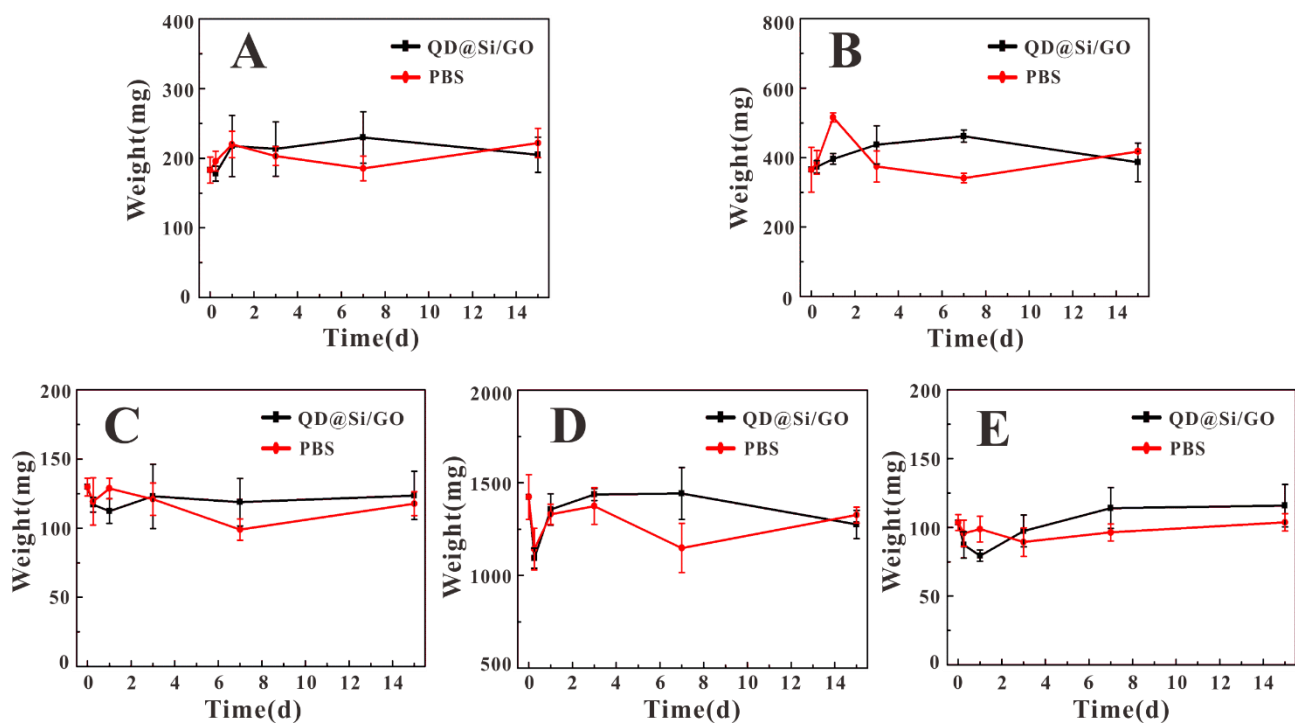


Fig. S11 Mass change in mouse lung (A), kidneys (B), heart (C), liver (D) and spleen (E) after probe injection, n = 5.

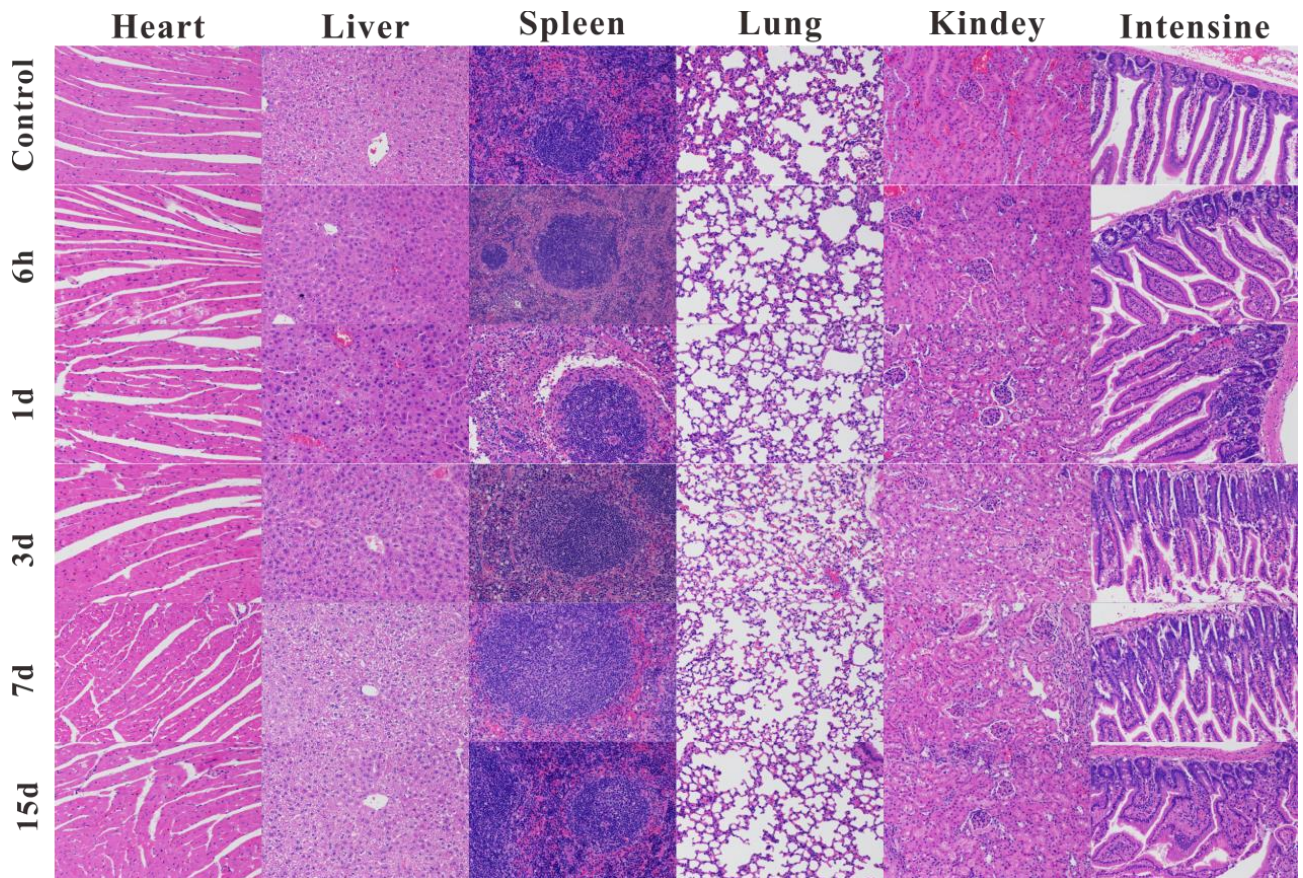


Fig. S12 H & E staining of heart, liver, spleen, lung, kidneys and small intestine of mice after intravenous injection of probe ($\times 200$).

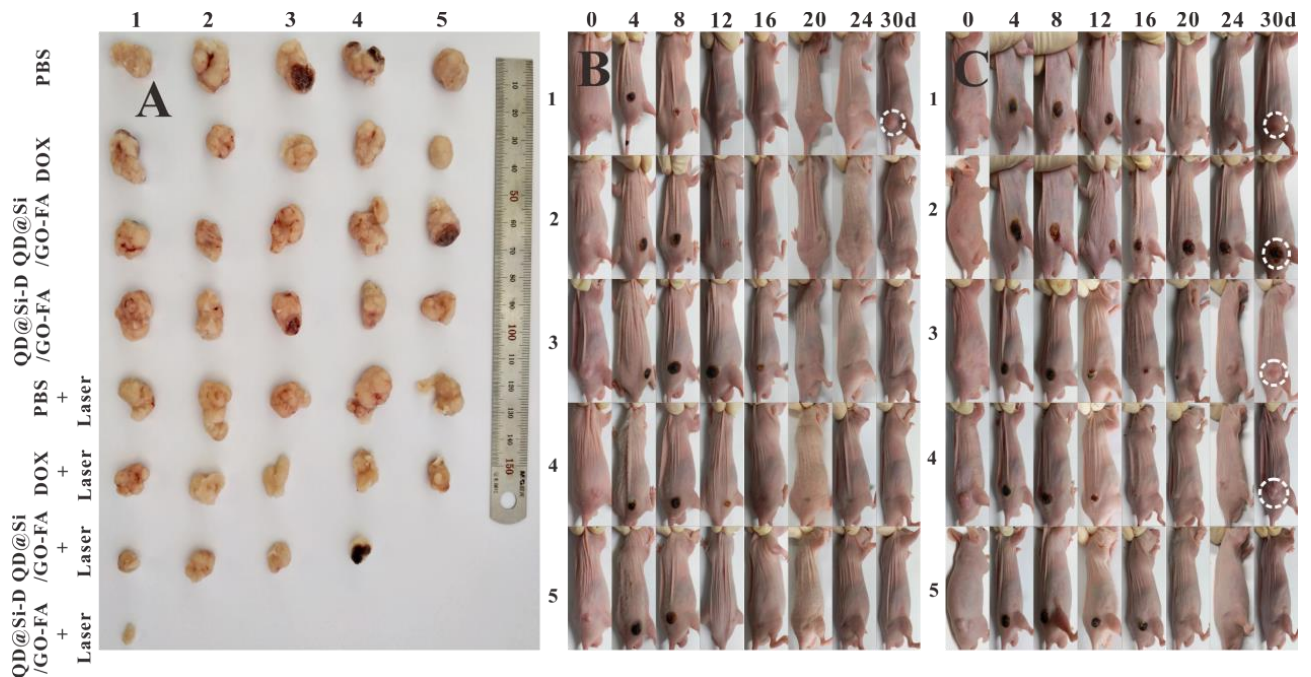


Fig. S13 Images of tumors of mice at the end of treatment (A); photographs of mice treated and relapsed after intravenous injection of QD@Si-D/GO-FA (B) and QD@Si/GO-FA (C).